

TEM investigation of interfaces during cuprous island growth

G.W. Zhou

Department of Mechanical Engineering and Multidisciplinary Program in Materials Science and Engineering, State University of New York, 4400 Vestal Parkway East, Binghamton, NY 13902, USA

Received 8 April 2009; received in revised form 4 June 2009; accepted 5 June 2009
Available online 3 July 2009

Abstract

The geometry and epitaxial relationships of interfaces generated during the early-stage oxidation of Cu(1 0 0) surfaces were studied using transmission electron microscopy. The predominant orientation relationship between Cu₂O islands and the Cu substrate is cube-on-cube growth, whereby equivalent planes and directions of oxide islands and the metal substrate are matched across the interface, while other epitaxies are occasionally observed. A 6 × 7 coincidence site lattice configuration is observed at the Cu–Cu₂O interface for the cube-on-cube epitaxy. The geometry of Cu₂O–Cu interfaces is found to depend on the specific epitaxial orientations of Cu₂O islands with the Cu substrate: wedge-shaped interfaces are developed for cube-on-cube growth, and edge-on interfaces are formed for other epitaxies. These growth features are attributed to the minimization of the interface energy via the competing factors among the coincidence lattice misfit, misfit dislocations and the metal–oxide interface area.

© 2009 Acta Materialia Inc. Published by Elsevier Ltd. All rights reserved.

Keywords: Transmission electron microscopy; Oxidation; Interface; Copper

1. Introduction

The oxidation of metals results in formation of various interfaces, including grain boundaries in the oxide scale and the metal–oxide interface. These interfaces play a critical role in oxide growth and can have a dramatic effect on the properties of the oxide scale. For example, the passivation behavior of metals is strongly influenced by the microstructures of the oxides that form. A large number of interfaces formed in the oxide scale often lead to poor oxidation resistance, because the outward diffusion of metal cations or inward diffusion of oxygen anions along these interfaces is probably much faster than that through a perfectly coalesced oxide film. However, point defects supporting diffusion during oxide growth are generated or annihilated at the metal–oxide interfaces, and the processes governing ionization and incorporation of metal atoms into the oxide phase are closely dependent on the

interface structure. Theoretical models on the effects of interface structure and the types and roles of interface defects in the growth of oxide scale have been developed [1–4]. Owing to their critical role in influencing oxide growth, there has also been extensive interest in experimental investigation of the atomic structure of metal–oxide interfaces. Transmission electron microscopy (TEM) is a powerful technique for probing local structures with high spatial resolution and has provided critical insight into understanding the atomic structures at metal–oxide interfaces for establishing the correlation between the interface structures and the mechanism of the oxidation of metals and alloys [5–16].

With the improvement in experimental techniques, especially with the development of in situ microscopy techniques, it is now possible to investigate early stages of metal oxidation. For instance, using a combination of in situ high-energy electron diffraction and TEM techniques, Milne and Howie studied early stages of Cu oxidation and observed the formation of Cu₂O islands from oxidation [17]. Yang et al. investigated the kinetics of early-stage oxidation of Cu surfaces

E-mail address: gzhou@binghamton.edu

with the use of in situ ultrahigh vacuum TEM to visualize oxide nucleation and growth [18–20]. These studies revealed that the oxidation of Cu results in nucleation of three-dimensional (3D) oxide islands on the metal surface which can grow and coalesce to form a continuous oxide film. Oxide islanding appears to be a common phenomenon for many pure metals such as Ni, Fe, Mo [21–23] and alloys such as Cu–Ni, Cu–Mn, Pd–Zn [5,10,11,24]. This work reports a detailed TEM study of the interface geometry, configuration and epitaxial relationships of Cu₂O nanoislands formed from the early-stage oxidation of Cu(1 0 0) thin films. Such information is needed for a better understanding of the oxidation mechanism of metals and alloys. Copper is of interest because of its wide industrial application. For example, copper is an attractive interconnect material for ultralarge scale integrated circuits because of its low resistivity and good electromigration properties [25], but it suffers from very poor oxidation resistance. The oxidation of copper has proved to be a rich source of information in understanding the corrosion of metals [17,26–36].

2. Experimental

The experimental system consists of single crystal, 70-nm-thick Cu(0 0 1) films grown epitaxially on freshly cleaved NaCl(0 0 1) substrates by sputter deposition at ~250 °C. The Cu films were removed from the substrate by flotation in deionized water, washed and mounted on a TEM Cu grid. The thickness of 70 nm of free-standing Cu films was chosen so that the films were thin enough to be examined by the TEM, but thick enough for oxidation behavior close to that of bulk metal. The single-crystallinity of the Cu films was checked by electron diffraction using TEM. The Cu films were first annealed at 700 °C in Ar–2% H₂ for 2 h to remove the native oxide. The Cu films were then oxidized at 700 °C in oxygen partial pressure (p_{O_2}) = 5×10^{-5} Torr for 5 min. TEM observations using a JEOL 2010F electron microscope were made immediately after removal of the oxidized samples from the oxidation chamber. TEM techniques including electron diffraction, high-resolution TEM (HRTEM), and electron moiré fringe imaging were used to determine the orientation relationships of oxide islands with the Cu substrate. TEM thickness fringe contrast was employed to analyze the interface geometry of interfaces associated with the oxide island growth. The advantage of using free-standing Cu thin films in the oxidation experiments is that the oxidized samples can be directly examined by TEM without additional TEM specimen processes, and the observed structure features correspond to the original state of the oxidized samples, greatly simplifying the link between experimental observation and the oxide growth mechanism.

3. Experimental results

Copper forms two thermodynamically stable oxides, Cu₂O and CuO. Cu₂O is simple cubic (space group $pn\bar{3}m$) with 4Cu and 2O atoms in its basis, and a lattice parameter

of 4.269 Å. The Cu atoms in Cu₂O form a face-centered cubic (fcc) lattice and the O atoms form a body-centered cubic (bcc) lattice, where each O atom is surrounded by a tetrahedron of Cu atoms. CuO has a monoclinic structure. Cu is a fcc metal with a lattice parameter of 3.61 Å. For the temperatures and low oxygen partial pressures used in these experiments, only Cu₂O is expected to form, which is also confirmed by electron diffraction.

Fig. 1 is a planar-view TEM image of an as-oxidized Cu thin film, revealing that the short-time oxidation of Cu[0 0 1] surfaces results in the formation of Cu₂O islands. The island lateral size varies from 200 to 500 nm, and the islands adopt a nearly square or polygon shape. It is noted in Fig. 1a that island 1 and island 2 are coalesced, and a grain boundary is formed between them. The different TEM contrast of islands 1 and 2 suggests that they have different crystallographic orientations with respect to the incidence electron beam. A selected-area diffraction (SAD) pattern from the rectangular enclosed area in Fig. 1a is given in Fig. 1b. Indexing of the diffraction pattern identified that one set of reflections is from island 1 and the other is from island 2, as illustrated in Fig. 1b, where 1 and 2 represent diffraction spots from island 1 and 2, respectively, and 1, 2 represents diffraction spots shared by island 1 and 2. Further analysis of the diffraction pattern indicates that the zone axis of island 1 is along [0 1 2], while the zone axis of island 2 is [0 0 1]. The absence of Cu diffraction spots in the diffraction pattern suggests that the Cu film beneath the oxide islands has been completely converted into Cu₂O. The orientation relationships of the two islands with the Cu substrate are determined as: $[0 1 2]_{\text{island-1}} \parallel [0 0 1]_{\text{Cu}}$ and $[0 0 1]_{\text{island-2}} \parallel [0 0 1]_{\text{Cu}}$. The orientation relationship between the two islands can be identified as: $(1 0 0)_{\text{island-1}} \parallel (1 0 0)_{\text{island-2}}$; $(0 2 \bar{1})_{\text{island-1}} \parallel (0 2 0)_{\text{island-2}}$ and $[0 1 2]_{\text{island-1}} \parallel [0 0 1]_{\text{island-2}}$. Since the orientation of the Cu film is along Cu[0 0 1], the orientation of island 2 with the Cu substrate can be identified as cube-on-cube epitaxy, under which equivalent planes and directions of oxide islands and the Cu substrate are matched across the metal–oxide interfaces. The electron diffraction analysis of different oxide islands revealed that most Cu₂O islands have the cube-on-cube orientation with the Cu substrate, and other epitaxies are observed only occasionally.

The metal–oxide interfaces were next examined for the growth of individual Cu₂O islands. Fig. 2a is a low-magnification dark-field (DF) TEM image of a Cu₂O island on a Cu(1 0 0) surface, where Cu(2 2 0) reflection was used for imaging. The oxide island shows a truncated-square shape. The oxide island has a cube-on-cube orientation with the Cu substrate. Note that oxide islands can develop from a nearly square shape to a truncated-square or irregular polygon shape with continued oxidation. The crystallographic direction of the island edges is identified by electron diffraction and is illustrated in Fig. 2a. The appearance of thickness fringe contrast around the island edges suggests that the Cu₂O island forms a wedge-shaped interface with the surrounding Cu film. This is because the

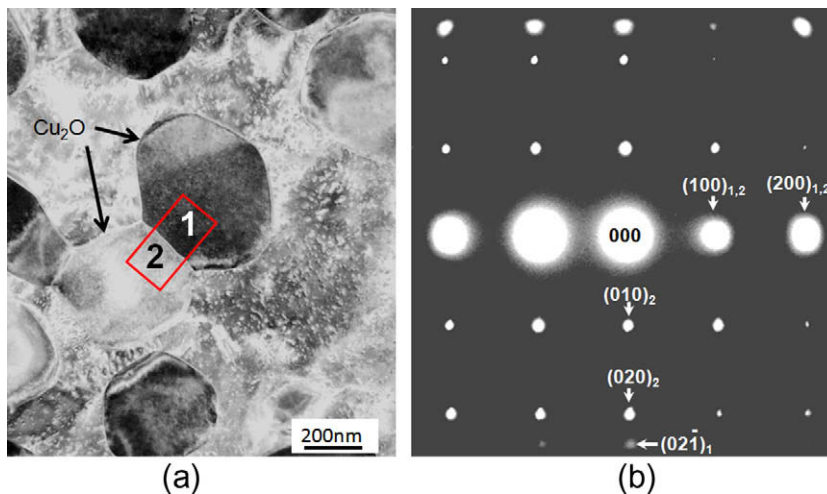


Fig. 1. (a) BF (bright field) TEM image of Cu_2O islands formed via oxidation of a $\text{Cu}(100)$ surface at 700°C ; island 1 and 2 are coalesced. (b) SAD pattern from the enclosed island area in (a); the zone axis of island 2 is along $[001]$ and has the cube-on-cube orientation with the Cu substrate, while the zone axis of island 2 is along $[012]$ and has non-cube-on-cube growth.

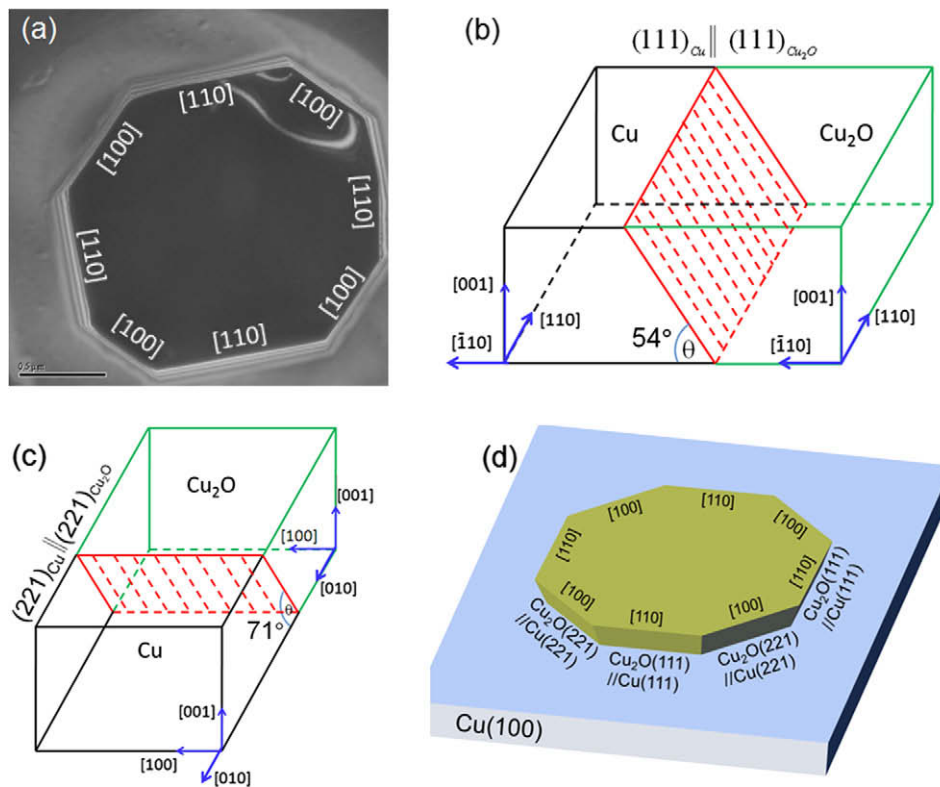


Fig. 2. (a) DF TEM image of one Cu_2O island using $\text{Cu}(220)$ reflection; thickness fringe contrast appears around the island edges. Note that $[100]$ and $[110]$ edges have different fringe spacings. (b) 3D schematic representation of the wedge-shaped interface along the $[110]$ edge: $(111)_{\text{Cu}_2\text{O}} \parallel (111)_{\text{Cu}}$. (c) 3D schematic representation of the wedge-shaped interface along the $[100]$ edge: $(221)_{\text{Cu}_2\text{O}} \parallel (221)_{\text{Cu}}$. (d) Schematic draw showing the 3D geometry of the buried part of the oxide island, where (111) and (221) denote the buried Cu_2O –Cu interfaces along the $[110]$ and $[100]$ island edges.

oxide growth is accompanied by conversion of the substrate atoms into the oxide phase along the metal–oxide interface, which causes the embedding of the oxide island into the Cu substrate and creates the wedge-shaped Cu– Cu_2O interfaces with continued oxide growth. As shown in Fig. 2a, the fringes' spacing depends on the orientation of the island edges. The spacing of the thickness fringes

along the four equivalent $[110]$ edges is equal but larger than that along the four equivalent $[100]$ edges, suggesting that the metal–oxide interfaces along the $[100]$ and $[110]$ edges have different interface geometries.

The fringe spacing can be measured directly from the TEM images, and this information is used to determine the interface shape. The thickness fringes for a DF image have

sinusoidal contrast variations. According to the Howie–Whelan equations [37], the intensity I from a diffracted beam g follows a sinusoidal variation for the DF image, which depends on the specimen thickness t , the extinction distance ξ_g , and the effective deviation parameter s_{eff} , where $s_{eff} = \sqrt{s^2 + \xi_g^{-2}}$, and s is the deviation parameter. For a wedge-shaped interface, the difference in the specimen thickness between two adjacent bright or dark lines is equal to the extinction distance ξ_g for Bragg diffraction conditions (i.e., $s = 0$). Here the g vector of $\text{Cu}(2\ 2\ 0)$ was used for forming the DF image, and $\xi_{\text{Cu}(2\ 2\ 0)} = 47.3$ nm for 100 keV electron beam [38]. The measured spacing of thickness fringes along $[1\ 1\ 0]$ edges is 33 nm. Therefore, the inclined angle of the interface with the Cu substrate can be determined as 54° , which is equal to the angle between the crystallographic planes $\text{Cu}(1\ 1\ 1)$ and $\text{Cu}(1\ 0\ 0)$. The schematic representation of this interface shape is illustrated in Fig. 2b, where the $(1\ 1\ 1)$ plane is the shared plane at the $\text{Cu}-\text{Cu}_2\text{O}$ interface, i.e., $(111)_{\text{Cu}_2\text{O}} \parallel (111)_{\text{Cu}}$. The shape of the interface along $[0\ 0\ 1]$ edges can be determined similarly and is illustrated in Fig. 2c. The measured spacing of thickness fringes along the $[1\ 0\ 0]$ edge is 16 nm, and the inclined angle of the interface with the Cu substrate is determined as 71° , which matches the angle between planes $(1\ 0\ 0)$ and $(2\ 2\ 1)$. Therefore, the interface along the $[1\ 0\ 0]$ edge is $(221)_{\text{Cu}_2\text{O}} \parallel (221)_{\text{Cu}}$. The TEM thickness fringe contrast analysis reveals that the buried part of the oxide island has

a pyramid shape, and a schematic representation of the shape of the buried island is given in Fig. 2d.

It is well known that moiré fringes can be formed in TEM images as a result of interference between diffracted beams from overlapping crystals [38–41]. Fig. 3a is a TEM micrograph from a $\text{Cu}-\text{Cu}_2\text{O}$ interface. A two-dimensional (2D) moiré pattern is present at the interface area, owing to the overlapping of Cu_2O and Cu lattices along the wedge-shaped $\text{Cu}_2\text{O}(1\ 1\ 1)/\text{Cu}(1\ 1\ 1)$ interface. Fig. 3b is a HRTEM image of the interface viewed from the $[0\ 0\ 1]$ zone axis. The left side of the HRTEM image corresponds to the Cu_2O phase, and its measured lattice spacing is 3.02 Å, which matches the interplanar spacings of $\text{Cu}_2\text{O}\{1\ 1\ 0\}$ planes. The right side of the HRTEM image corresponds to Cu lattice, and the measured lattice spacing is 2.55 Å, consistent with the interplanar spacing of $\text{Cu}\{1\ 1\ 0\}$ planes. As can be seen from the HRTEM image, the Cu_2O and Cu lattices have the cube-on-cube orientation at the interface, i.e., the equivalent planes and directions of Cu and Cu_2O are matched across the interface: $(110)_{\text{Cu}_2\text{O}} \parallel (110)_{\text{Cu}}$, $(1\bar{1}0)_{\text{Cu}_2\text{O}} \parallel (1\bar{1}0)_{\text{Cu}}$, and $[001]_{\text{Cu}_2\text{O}} \parallel [001]_{\text{Cu}}$. Considering that a fringe moiré pattern is produced by a single set of parallel overlapping Cu_2O and Cu lattice planes, the two intersecting moiré fringes appearing in the moiré pattern in Fig. 3a and b suggests that there are two sets of parallel overlapping Cu_2O and Cu planes in the interface region, and each set is rotated with respect to the other by 90° . The formation of this

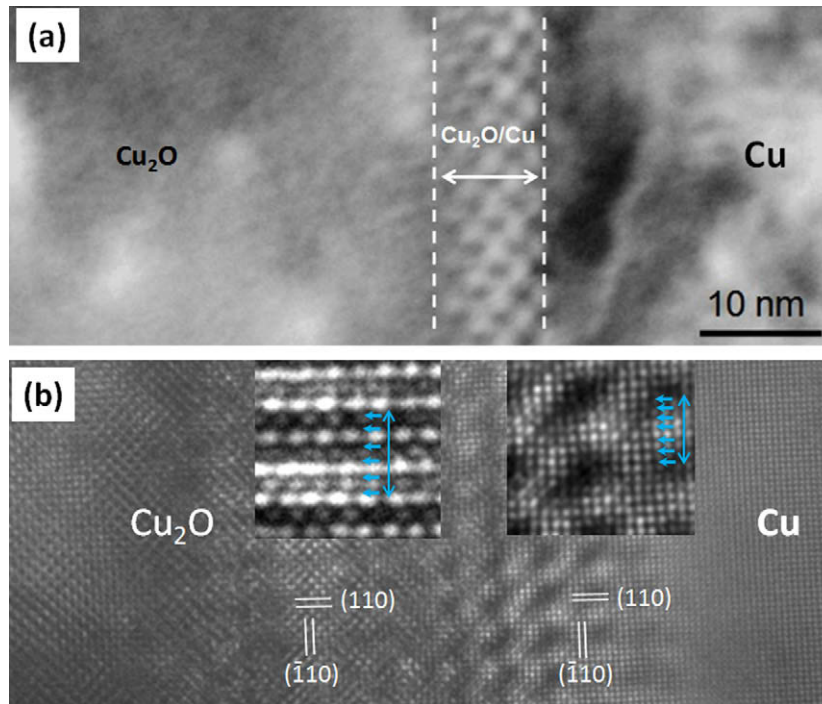


Fig. 3. (a) BF TEM image depicting the 2D moiré fringe pattern at the $\text{Cu}_2\text{O}-\text{Cu}$ interface along the $[1\ 1\ 0]$ edge. (b) A $[0\ 0\ 1]$ viewed HETEM image of the $\text{Cu}_2\text{O}-\text{Cu}$ interface revealing the epitaxial orientations between Cu_2O and Cu lattices; left inset: an enlarged HRTEM image from the interface region closer to the Cu_2O lattice side, which reveals that each moiré repeat contains six $\text{Cu}_2\text{O}(1\ 1\ 0)$ planes; right inset: an enlarged HRTEM image from the interface region closer to the Cu lattice side, where each moiré repeat contains seven $\text{Cu}(1\ 1\ 0)$ planes.

2D moiré pattern is caused by the wedge-shaped interface with the identified epitaxial relationships as well as the zone axis incidence (i.e., $[0\ 0\ 1]$) of the electron beam.

The contribution to the moiré fringe contrast in the HRTEM image in Fig. 3b comes from double diffraction of $\text{Cu}_2\text{O}(2\ 0\ 2)$ and $\text{Cu}(2\ 0\ 2)$ reflections because of the systematic absence of $\text{Cu}(1\ 0\ 1)$ reflection. Given the interplanar spacings d_1 and d_2 of two overlapping crystals, the spacing of parallel moiré fringes D can be calculated by $D = d_1 d_2 / (d_1 - d_2)$. Using the measured spacings of $\text{Cu}(1\ 1\ 0)$ and $\text{Cu}_2\text{O}(1\ 1\ 0)$, the spacing D of $\{2\ 2\ 0\}$ moiré fringes should be 8.2 Å, which is equal to the spacing of the moiré repeat measured from the HRTEM image (Fig. 3b). The moiré repeat width of 8.2 Å is also equal to the spacing obtained using the bulk lattice parameters of Cu_2O and Cu, suggesting that the Cu_2O and Cu lattice have a nearly stress-free interface configuration.

The natural lattice misfit between Cu and Cu_2O is 15.4%. This large lattice misfit makes the formation of coherently strained metal–oxide interfaces energetically unfavorable. It has been suggested that the occurrence of epitaxy in large-misfit systems is related to the formation of a near coincidence site lattice (CSL) interface configuration requiring lattice strains small enough to be energetically feasible [42–45]. In this case, the bilayer would be in a local minimum energy state if the m th atom of the overgrowth coincides with the n th atom of the substrate by introducing a minimum lattice misfit

$$F = -(ma_o - na_s) / ma_o \quad (1)$$

where m and n can be predicted from the relation $a_o/a_s = m/n$ of the unstrained lattice parameters of the overlayer a_o and the substrate a_s and $n = m \pm 1$ [46–48]. For the Cu_2O –Cu system, a 6×7 CSL has been proposed, because it provides a minimum coincidence misfit of $F_0 = 1.22\%$ [35,49]. This 6×7 CSL interface configuration can be confirmed from the inset HRTEM images in Fig. 3b. The periodicity of the moiré fringes on the Cu side reveals that each moiré repeat contains seven $\text{Cu}(1\ 1\ 0)$ spacings, and the moiré repeat on the Cu_2O side contains six $\text{Cu}_2\text{O}(1\ 1\ 0)$ spacings.

In addition to the cube-on-cube epitaxy, interfaces with other epitaxies are observed occasionally, where the matched lattices across the metal–oxide interface are not equivalent parallel planes and directions of Cu and Cu_2O . Surprisingly, rather than forming the inclined interfaces as observed for the cube-on-cube growth, these non-cube-on-cube epitaxies result in edge-on Cu_2O –Cu interfaces. Fig. 4a is an HRTEM image from an edge-on interface, where the Cu side has the zone axis of $\text{Cu}[0\ 0\ 1]$ parallel to the incident e-beam, and 2D lattice is visible, while the Cu_2O side shows only one-dimensional lattice. The SAD pattern in Fig. 4b is from the Cu_2O side, and its zone axis is along $\text{Cu}_2\text{O}[\bar{1}\ \bar{1}\ 2]$. The combined HRTEM image and electron diffraction reveal that the epitaxial relationship of the Cu_2O and Cu lattices is $(111)_{\text{Cu}_2\text{O}}$

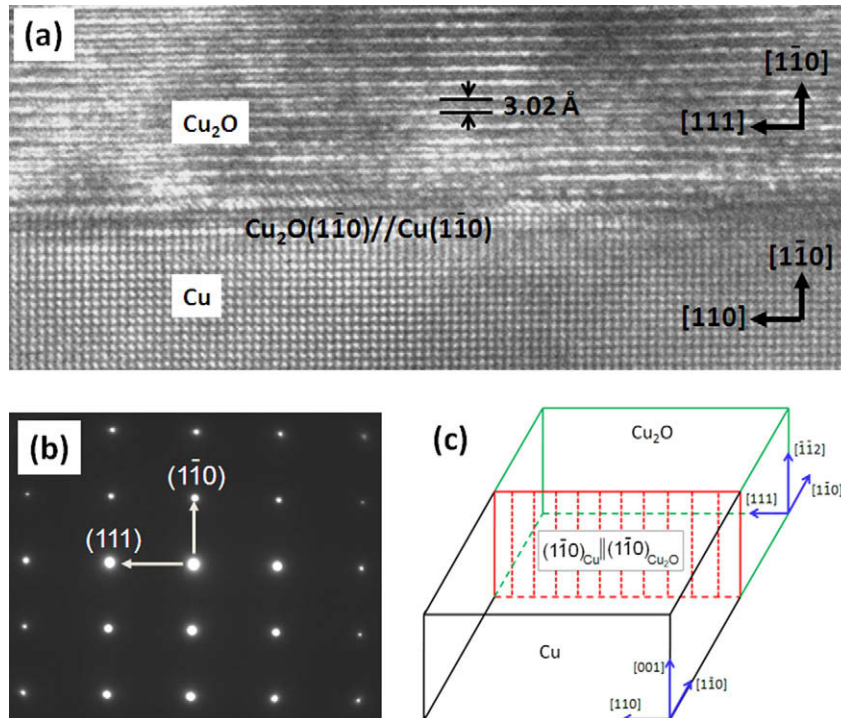


Fig. 4. (a) HRTEM image showing an edge-on Cu_2O –Cu interface, where the orientation relationship of the Cu_2O and Cu lattices is not cube-on-cube. The shared plane at the Cu_2O –Cu interface is $(1\ \bar{1}\ 0)_{\text{Cu}_2\text{O}} \parallel (1\ \bar{1}\ 0)_{\text{Cu}}$. The absence of moiré fringe contrast at the interface region suggests that it is an edge-on interface. (b) SAD pattern from the Cu_2O region in (a); the epitaxial orientation of the Cu_2O with respect to the Cu substrate is $(111)_{\text{Cu}_2\text{O}} \parallel (110)_{\text{Cu}}$, $(1\ \bar{1}\ 0)_{\text{Cu}_2\text{O}} \parallel (1\ \bar{1}\ 0)_{\text{Cu}}$, and $[\bar{1}\ \bar{1}\ 2]_{\text{Cu}_2\text{O}} \parallel [001]_{\text{Cu}}$. (c) Schematic 3D representation of the interface geometry.

$\|(110)_{\text{Cu}}, (1\bar{1}0)_{\text{Cu}_2\text{O}}\|(1\bar{1}0)_{\text{Cu}}$ and $[\bar{1}12]_{\text{Cu}_2\text{O}}\|[001]_{\text{Cu}}$. It is worth noticing that no moiré fringe contrast is present near the interface zone, suggesting that the Cu_2O and Cu lattices are aligned edge-on at the interface. The HRTEM image in Fig. 4a indicates that the Cu_2O and Cu lattices are joined along the planes of $(1\bar{1}0)_{\text{Cu}_2\text{O}}\|(1\bar{1}0)_{\text{Cu}}$. Fig. 4c is a 3D schematic representation of this interface geometry.

Fig. 5a shows another example of edge-on Cu_2O –Cu interfaces. Again, the absence of moiré fringes contrast near the interface zone confirms that it is an edge-on interface. The HRTEM image indicates that the Cu region has the zone axis $\text{Cu}[001]$ parallel to the incident electron beam. The electron diffraction shown in Fig. 5b was taken from the oxide region, and the zone axis of the Cu_2O region is identified as $\text{Cu}_2\text{O}[\bar{1}12]$. So the epitaxial relations between the Cu_2O island and the Cu film are identified as $(1\bar{1}1)_{\text{Cu}_2\text{O}}\|(1\bar{1}0)_{\text{Cu}}, (110)_{\text{Cu}_2\text{O}}\|(110)_{\text{Cu}}$ and $[\bar{1}12]_{\text{Cu}_2\text{O}}\|[001]_{\text{Cu}}$. As shown in the HRTEM image in Fig. 5a, the Cu_2O –Cu interface formed for this epitaxial orientation adopts a high Miller index plane which is identified as $(320)_{\text{Cu}_2\text{O}}\|(320)_{\text{Cu}}$ by measuring the contact angle of the interface with the low-index (110) planes of both the Cu and Cu_2O lattices. Fig. 5c shows a 3D schematic representation of this interface shape.

4. Discussion

Two questions are raised by the TEM characterization of the interface structure and geometry for the Cu_2O island

growth: (1) Why is the cube-on-cube growth the major type of orientation? (2) Why does the cube-on-cube growth favor inclined interface geometries, while others prefer edge-on interface geometries? It is reasonable to expect that these different interface geometries have different interfacial structures and therefore different interface energy. A minimum energy criterion is used to predict the thermodynamically favorable epitaxial relationships between the oxide and the metal substrate, and they are compared with the experimental results.

The interface energy per unit area of an elastically strained interface layer is

$$E_{el} = 2G \frac{1+v}{1-v} \varepsilon^2 h \quad (2)$$

where G is the shear modulus of the oxide, v is the Poisson's ratio, ε is the elastic strain in the oxide, and h is the thickness of the interfacial layer. The generation of misfit dislocations at the interface causes additional energy by [50]

$$E_d = \frac{Gb(F-\varepsilon)}{2\pi(1-v)} \left[\ln\left(\frac{h}{b}\right) + 1 \right] \quad (3)$$

where F is the coincidence misfit, and b is the edge component of the Burgers vector of misfit dislocations. The total energy per unit area can be written as

$$E = E_{el} + E_d = \frac{2G(1+v)}{1-v} \varepsilon^2 h + \frac{Gb|F-\varepsilon|}{2\pi(1-v)} \left[\ln\left(\frac{h}{b}\right) + 1 \right] \quad (4)$$

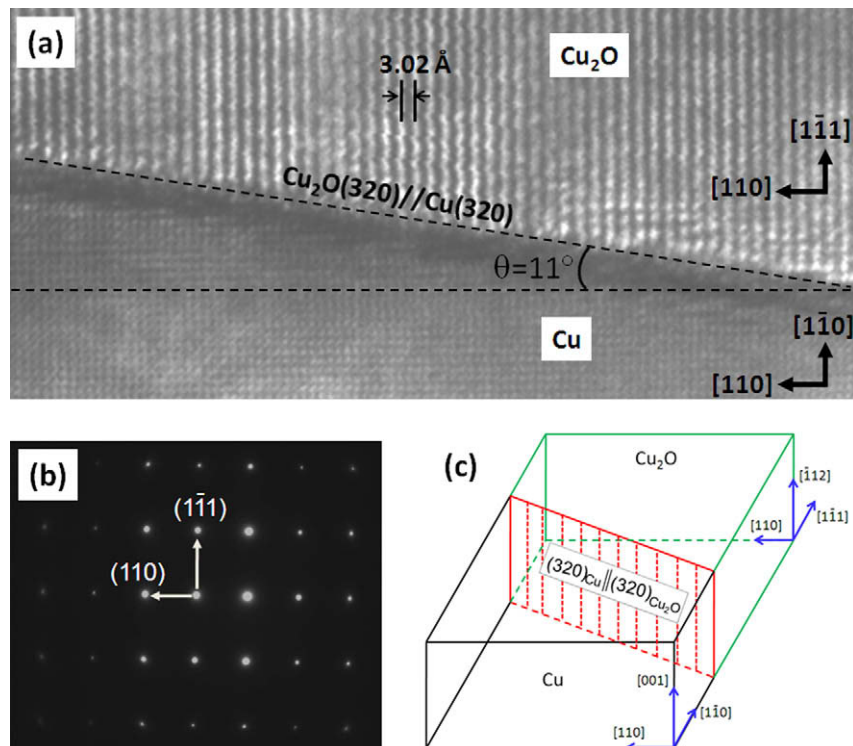


Fig. 5. (a) HRTEM image showing an edge-on interface with the shared plane of $(320)_{\text{Cu}_2\text{O}}\|(320)_{\text{Cu}}$; the absence of moiré fringes at the interface area implies that it is an edge-on interface. (b) SAD pattern from the Cu_2O region in (a), the epitaxial orientation of the Cu_2O island with respect to the Cu substrate is $(1\bar{1}1)_{\text{Cu}_2\text{O}}\|(1\bar{1}0)_{\text{Cu}}, (110)_{\text{Cu}_2\text{O}}\|(110)_{\text{Cu}}$, and $[\bar{1}12]_{\text{Cu}_2\text{O}}\|[001]_{\text{Cu}}$. (c) Schematic 3D representation of the interface geometry.

The magnitude of the elastic strain ε^* at which a minimum total energy E^* can be obtained by setting $\partial E/\partial \varepsilon = 0$ is given by

$$|\varepsilon|^* = \frac{b}{8\pi(1+\nu)h} \left[\ln \left(\frac{h}{b} \right) + 1 \right] \quad (5)$$

Based on the above derivation, the selection of the epitaxial relationship and interface geometry during the oxide island growth can now be discussed. It can be easily noted from expressions (4) and (5) that E^* increases linearly with increasing coincidence misfit F . According to the epitaxy theories for large-misfit growth [42,45–48,50], the interface configuration with $a_o/a_s = m/n$ and $n = m \pm 1$ provides a minimum coincidence misfit F , where a_o and a_s are the lattice constants of the oxide and the metal substrate, and F can be calculated using Eq. (1). For Cu–Cu₂O system, both crystals belong to the cubic system, and the cubic-on-cube growth produces a 6×7 CSL interface configuration in which six Cu spacings in the Cu₂O overlayer exactly match seven Cu spacings in the Cu substrate with a minimum coincidence misfit $F = 1.22\%$. Any other epitaxies will cause a larger coincidence misfit and therefore increase the equilibrium energy E^* . This explains why the epitaxial relationship is dominated by the cube-on-cube growth.

The correlation between the interface geometry and the equilibrium energy E^* is now discussed. As Eqs. (4) and (5) show, the equilibrium energy E^* also depends on the magnitude of the Burgers vector \mathbf{b} of the misfit dislocations. Unlike the dislocations in the bulk, the misfit dislocations at the metal–oxide interfaces are not defects but an integral part of the interface structure [10,11]. Taking a geometrical approach based on Bollmann's O-lattice theory [48], a CSL interface can be divided into coherent regions that are separated by regions of disturbed coherency, which are assumed to relax by misfit dislocations. For the parallel (1 1 1) interfaces of Cu₂O and Cu with the cube-on-cube orientation relationship, hexagonal or trigonal networks of misfit dislocations can be constructed. The most effective dislocations accommodating lattice mismatch for the (1 1 1) interfaces are edge dislocations with a Burgers vector $1/2\langle 110 \rangle$ along the $\langle 211 \rangle$ dislocation line direction, using the coherent interface as the reference system [10,11,48]. Alternatively, an edge dislocation network of partial dislocations with a Burgers vector $1/6\langle 211 \rangle$ along the $\langle 110 \rangle$ line direction can be assumed on the (1 1 1) interface. Similarly, for the (2 2 1) interface of Cu₂O and Cu with the cube-on-cube growth, edge dislocations with a Burgers vector of $1/2\langle 110 \rangle$ along $\langle 211 \rangle$ line direction can be also obtained. These relations explain why the inclined (111)_{Cu₂O} || (111)_{Cu} and (221)_{Cu₂O} || (221)_{Cu} interface geometries are favored by the cube-on-cube growth, because these two interface geometries provide the most effective edge dislocations accommodating the lattice mismatch.

Epitaxies other than the cube-on-cube growth are less frequently observed, because they are less energetically favorable. Although non-cube-on-cube growth produces

a larger coincidence misfit, the oxide island can adjust the growth morphology and develop into interface geometry with a minimum metal–oxide interfacial area, thereby reducing the total interfacial energy. This explains why an edge-on interface shape is adopted for non-cube-on-cube growth, because the edge-on interface geometry offers the smallest interface area compared with inclined interface geometries, and therefore partially offsets the increased interfacial strain energy due to larger coincidence lattice misfits associated with the non-cube-on-cube oxide growth.

5. Conclusions

The geometry and epitaxial relationships of interfaces formed during the early-stage oxidation of Cu(1 0 0) thin films were investigated. The major findings include:

1. The orientation relationship between Cu₂O islands and the Cu substrate is dominated by cube-on-cube growth, and other epitaxies are occasionally observed.
2. For cube-on-cube growth, a wedge-shaped interface is developed; for other epitaxies, an edge-on interface is formed.
3. A 6×7 CSL interface configuration is developed at the Cu–Cu₂O interface for cube-on-cube epitaxy.

These growth features can be attributed to thermodynamic factors. The cube-on-cube orientation provides a minimum CSL misfit, thereby minimizing the interfacial energy, and therefore dominates the epitaxial relationship of oxide islands with the substrate. The formation of inclined Cu₂O–Cu interfaces associated with the cube-on-cube growth is due to these interface geometries providing the most effective misfit dislocations accommodating the lattice misfit. The increased lattice misfit caused by non-cube-on-cube growth can be partially offset by the formation of edge-on interfaces that minimize the total interface area, thereby reducing the total interface energy. Since oxide islanding during oxidation has been observed for many metals, including Fe, Pd, Ni, Co, Ti, Pb and Sn, as well as Cu, it is expected that these results may have a broader impact for manipulating metal oxidation to affect the reaction product morphology and perhaps the oxidation kinetics.

Acknowledgements

The author gratefully acknowledges the reviewer for insightful suggestions, which have significantly improved the manuscript. The research was supported by the National Science Foundation (NSF) under Grant CMMI-0825737.

References

- [1] Hirth JP, Mitchell TE. Acta Mater 2008;56:5701.
- [2] Pieraggi B, Rapp RA. Acta Metallurg 1988;36:1281.

- [3] Pieraggi B, Rapp RA, Hirth JP. *Oxidation Metals* 1995;44:63.
- [4] Hirth JP, Pond RC. *Acta Mater* 1996;44:4749.
- [5] Groen HB, De Hosson JTM. *Scripta Mater* 1998;38:769.
- [6] Groen HB, Kooi BJ, Vellinga WP, De Hosson JTM. *Philos Mag A* 1999;79:2083.
- [7] Kooi BJ, De Hosson JTM. *Acta Mater* 1998;46:1909.
- [8] Kooi BJ, Groen HB, De Hosson JTM. *Acta Mater* 1997;46:112.
- [9] Kooi BJ, Groen HB, De Hosson JTM. *Acta Mater* 1997;45:3587.
- [10] De Hosson JTM, Groen HB, Kooi BJ, Vitek V. *Acta Mater* 1999;47:4077.
- [11] De Hosson JTM, Kooi BJ. *Surf Interf Anal* 2001;31:637.
- [12] Reichel F, Jeurgens LPH, Richter G, Mittemeijer EJ. *J Appl Phys* 2008;103:093515.
- [13] Reichel F, Jeurgens LPH, Richter G, van Aken PA, Mittemeijer EJ. *Acta Mater* 2007;55:6027.
- [14] Jeurgens LPH, Sloof WG, Tichelaar FD, Mittemeijer EJ. *Thin Solid Films* 2002;418:89.
- [15] Ruhle M. *J Eur Ceram Soc* 1996;16:353.
- [16] Yang JC, Schumann E, Mulleijans H, Ruhle M. *J Phys D Appl Phys* 1996;29:1716.
- [17] Milne RH, Howie A. *Philos Mag A* 1984;49:665.
- [18] Yang JC, Evan D, Tropa L. *Appl Phys Lett* 2002;81:241.
- [19] Yang JC, Yeadon M, Kolasa B, Gibson JM. *Scripta Mater* 1998;38:1237.
- [20] Geng YJ, Norton MG. *J Mater Res* 1999;14:2708.
- [21] Holloway PH, Hudson JB. *Surf Sci* 1974;43:123.
- [22] Aggarwal S, Monga AP, Perusse SR, Ramesh R, Ballarotto V, Williams ED, et al. *Science* 2000;287:2235.
- [23] Lawless KR. *Rep Prog Phys* 1974;37:231.
- [24] Hajcsar EE, Underhill PR, Smeltzer WW. *Langmuir* 1995;11:4862.
- [25] Ohba T. *Appl Surf Sci* 1995;91:1.
- [26] Yang JC, Kolasa B, Gibson JM, Yeadon M. *Appl Phys Lett* 1998;73:2841.
- [27] Eastman JA, Fuss PH, Rehn LE, Baldo PE, Zhou GW, Fong DD, et al. *Appl Phys Lett* 2005;87:051914.
- [28] Zhou GW, Chen XD, Gallagher D, Yang JC. *Appl Phys Lett* 2008;93:123104.
- [29] Zhou GW, Yang JC. *Phys Rev Lett* 2002;89:106101.
- [30] Zhou GW, Slaughter WS, Yang JC. *Phys Rev Lett* 2005;94:246101.
- [31] Lahtonen K, Hirsimäki M, Lampimäki M, Valden M. *J Chem Phys* 2008;129:124703.
- [32] Verma SK, Raynaud GM, Rapp RA. *Oxidation Metals* 1981;11:471.
- [33] Raynaud GM, Rapp RA. *Oxidation Metals* 1984;21:89.
- [34] Zhou GW, Yang JC. *Appl Surf Sci* 2003;210:165.
- [35] Ho JH, Vook RW. *J Cryst Growth* 1978;44:561.
- [36] Ho JH, Vook RW. *Philos Mag A* 1977;36:1051.
- [37] Hirsch PB, Howie A, Nicholson RB, Pashley DW, Whelan MJ. *Electron microscopy of thin crystals*. New York: Krieger; 1977.
- [38] Williams DB, Carter CB. *Transmission electron microscopy*. New York: Plenum; 1996.
- [39] Fultz B, Howe JM. *Transmission electron microscopy and diffraction in materials science*. Berlin: Springer; 2001.
- [40] Li BQ, Zuo JM. *Surf Sci* 2002;520:7.
- [41] Li BQ, Zuo JM. *J Appl Phys* 2003;94:743.
- [42] Fletcher NH, Lodge KW. In: Matthews JW, editor. *Epitaxial growth, Part B*. New York: Academic Press; 1975. p. 529.
- [43] Dahmen U. *Acta Metallurg* 1982;30:63.
- [44] Salles-Desvignes I, Montesin T, Valot C, Bertrand G, Vadon A. *Acta Mater* 2000;48:1505.
- [45] Du Plessis JC, Van der Merwe JH. *Philos Mag* 1965;11:43.
- [46] Matthews JW. In: Nabarro FRN, editor. *Dislocations in solids*. Amsterdam: North-Holland; 1979. p. 462.
- [47] Fletcher N, Adamson PL. *Philos Mag* 1966;13:99.
- [48] Bollmann W. *Crystal defects and crystalline interfaces*. New York: Springer-Verlag; 1970.
- [49] Chu YS, Robinson IK, Gewirth AA. *J Chem Phys* 1999;110:5952.
- [50] Matthews JW. In: Matthews JW, editor. *Epitaxial growth, Part B*. New York: Academic Press; 1975.